

Magnetic phase transitions in two-dimensional two-valley semiconductors with in-plane magnetic field

Dmitry Miserev, Jelena Klinovaja, and Daniel Loss¹

¹*Department of Physics, University of Basel, Klingelbergstrasse 82, CH-4056 Basel, Switzerland*
(Dated: August 18, 2020)

A two-dimensional electron gas (2DEG) in two-valley semiconductors has two discrete degrees of freedom given by the spin and valley quantum numbers. We analyze the zero-temperature magnetic instabilities of two-valley semiconductors with SOI, in-plane magnetic field, and electron-electron interaction. The interplay of an applied in-plane magnetic field and the SOI results in non-collinear spin quantization in different valleys. Together with the exchange intervalley interaction this results in a rich phase diagram containing four non-trivial magnetic phases. The negative non-analytic cubic correction to the free energy, which is always present in an interacting 2DEG, is responsible for first order phase transitions. Here, we show that non-zero ground state values of the order parameters can cut this cubic non-analyticity and drive certain magnetic phase transitions second order. We also find two tri-critical points at zero temperature which together with the line of second order phase transitions constitute the quantum critical sector of the phase diagram. The phase transitions can be tuned externally by electrostatic gates or by the in-plane magnetic field.

Introduction. Modern nanotechnology is mostly based on layered quantum materials where electrons or holes are confined within one layer which makes them effectively two-dimensional (2D) [1]. The 2D layers are typically represented by semiconductors such as GaAs, InAs, and InSb which are single valley materials meaning that the electron energy has a single minimum in the Brillouin zone [2]. Bulk Si and Ge have a valley degree of freedom, i.e. their bulk spectrum has several minima in the Brillouin zone (six for Si and four for Ge) [3]. In thin Ge films the valley degeneracy is lifted [3], while it survives in a Si 2D electron gas (2DEG). This results in qualitatively new physics in Si 2DEGs that has no analogues in single-valley 2DEGs. For example, the valley degeneracy in Si 2DEGs allows for the singlet-triplet level crossing in 2D two-electron Si quantum dots [4], an effect which is forbidden in single-valley materials [5]. However, the spectrum of Si 2DEG still has a single minimum in 2D Brillouin zone. A new class of 2D semiconductors with the electron spectrum containing two distinct minima (see Fig. 1) is represented by monolayers of transition metal dichalcogenides (TMD) [6, 7]. These spectral minima are separated by a wave vector \mathbf{q}_0 , which is in order of the Brillouin zone momentum, $|\mathbf{q}_0| \sim 1/a_0$, a_0 being the lattice constant.

Magnetic instabilities in monolayers of TMDs were analyzed theoretically in Refs. [8–11]. Mixed ferromagnetic and valley polarized phases are predicted in the spin locking regime when the spin-orbit interaction (SOI) is much larger than the Fermi energy E_F , the regime that is realistic for the hole doped TMDs [8, 9] where the SOI gap is in order of few hundred meV [12–15]. The opposite limit of small SOI compared to E_F was considered in Refs. [10, 11] and is relevant for electron doped monolayers of TMDs, especially for MoS₂ which has the smallest SOI gap ~ 3 meV among all monolayer TMDs [16–22]. The exchange intervalley interaction and the dynam-

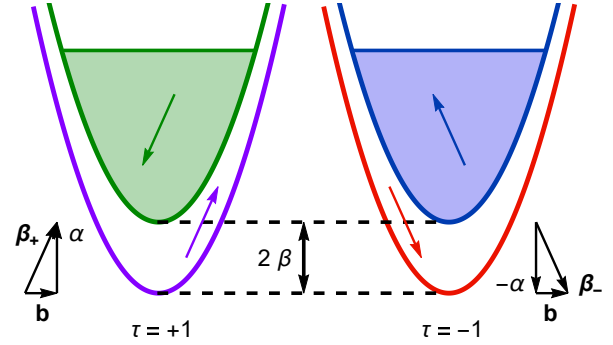


FIG. 1. Electron spectrum in presence of the valley SOI and the in-plane magnetic field, see Eq. (4). Valleys are indicated by the index $\tau = \pm 1$. The spin degeneracy in each valley is lifted by the gap 2β , see Eq. (4). The spin quantization axis in $\tau = +1$ ($\tau = -1$) valley is directed along β_+ (β_-), see Eq. (3), corresponding spin projections are shown by arrows. Here we show an example of equal filling of green and blue bands, while purple and red bands are unfilled due to the effect of electron-electron interaction. Such filling corresponds to the phase I', see Fig. 2, with $M_v = M_{\beta v} = 0$, $M_\beta \neq 0$, see Eq. (S39).

ical screening of the Coulomb interaction are omitted in Ref. [10]. It was then shown subsequently [11] that these two ingredients have a dramatic effect on the magnetic phase diagram of TMDs. In particular, finite exchange intervalley interaction favors a ferromagnetic instability and biases out other possible magnetic orders. The phase transition between the ferromagnetic and the paramagnetic ground states of the 2DEG is predicted to be of first order due to the dynamical screening of the Coulomb interaction by gapless electron-hole fluctuations [23]. The theoretical results [11] agree well with recent experiments on electron doped monolayer MoS₂ [24–26].

Here, we study the effect of an applied in-plane magnetic field on the magnetic phase diagram of 2D two-valley semiconductors such as electron doped monolayer

TMDs, see Fig. 1. This effect has not been studied theoretically so far and leads to a rather rich magnetic phase diagram allowing for the phase transitions to be driven not only by the electron density, which is tunable by electrostatic gates, but also by the external magnetic field. In this work we do not consider out-of-plane magnetic fields to avoid complications related to Landau quantization. We also assume that the SOI is much smaller than E_F of the 2DEG in the normal phase. Together with the intrinsic SOI the in-plane magnetic field leads to a non-collinear spin quantization in different valleys which are coupled by exchange intervalley interaction. This breaks spin conservation which has a dramatic effect on the magnetic phase diagram. Indeed, we show that four non-trivial magnetic orders are possible. The phase transitions between the different phases can be driven by changing the electron density and the external in-plane magnetic field.

In order to study the order of a phase transition, we calculate the non-analytic cubic correction to the free energy of the 2DEG which comes from the dynamical screening of the Coulomb interaction and from the interaction vertex correction due to gapless electron-hole fluctuations [23]. In case of a single magnetic order parameter (spin magnetization) the non-analytic cubic term is always negative [27] which results in a first order ferromagnetic phase transition at small temperatures [23, 28]. The finite temperature [29] or finite SOI [30, 31] gap out the electron-hole continuum which is known to drive a second order magnetic phase transition [32]. However, the valley degree of freedom in two-valley semiconductors results in three independent magnetic order parameters that are coupled together via the non-analytic cubic correction. The cubic correction is negative as in the case of a single magnetic order parameter. However, we show that certain phase transitions are of second order due to the interplay between all three order parameters coupled by the non-analytic cubic correction. We also identify two tri-critical points on the zero-temperature phase diagram that together with the line of second order phase transitions represent the quantum critical sector.

Single-particle spectrum. The single-particle spectrum of a 2D two-valley semiconductor can be described by the following effective Hamiltonian [21]:

$$H = \frac{\mathbf{k}^2}{2m} - \alpha\sigma_z\tau - g\mu_B\mathbf{B} \cdot \frac{\boldsymbol{\sigma}}{2}, \quad (1)$$

where $\mathbf{k} = (k_x, k_y)$ is the in-plane momentum, m the effective electron mass, α the valley SOI, g the electron g -factor, μ_B the Bohr magneton, $\mathbf{B} = (B_x, B_y, 0)$ the in-plane magnetic field, $\boldsymbol{\sigma} = (\sigma_x, \sigma_y, \sigma_z)$ the Pauli matrices corresponding to the electron spin, and $\tau = \pm 1$ labels the two valleys. The valley SOI acts as an effective out-of-plane magnetic field taking opposite signs in different valleys. Thus, the effective single-particle Hamiltonian (1) can be represented as a Zeeman Hamiltonian with a

valley-dependent effective magnetic field $\boldsymbol{\beta}_\tau$:

$$H = \frac{\mathbf{k}^2}{2m} - \boldsymbol{\beta}_\tau \cdot \boldsymbol{\sigma}, \quad (2)$$

$$\boldsymbol{\beta}_\tau = (b_x, b_y, \alpha\tau), \quad \mathbf{b} = g\mu_B \frac{\mathbf{B}}{2}. \quad (3)$$

The free-electron spectrum described by Eq. (2), thus consists of two pairs of parabolic energy bands (one pair per valley) each of which is split by the corresponding effective magnetic field $\boldsymbol{\beta}_\tau$, see Fig. 1:

$$\varepsilon_\tau^\lambda(k) = \frac{k^2}{2m} - \lambda\beta, \quad \beta = |\boldsymbol{\beta}_\tau| = \sqrt{\alpha^2 + b^2}, \quad (4)$$

where $\lambda = \pm 1$ is the eigenvalue of the operator $\boldsymbol{\beta}_\tau \cdot \boldsymbol{\sigma}/\beta$, $k^2 = k_x^2 + k_y^2$, $b = |\mathbf{b}| = \sqrt{b_x^2 + b_y^2}$. As $|\boldsymbol{\beta}_+| = |\boldsymbol{\beta}_-| = \beta$, the single-particle spectrum is doubly degenerate. The electron spin in valley τ is quantized along the direction $\boldsymbol{\beta}_\tau/\beta$ of the effective magnetic field $\boldsymbol{\beta}_\tau$, see Fig. 1.

Magnetic order parameters. In absence of interactions the chemical potential is the same for all single-particle bands, see Eq. (4). We refer to this ground state as normal state. Sufficiently strong electron-electron interactions may result in unequal chemical potentials for different single-particle bands. For example, strong electron-electron interaction in a single-valley 2DEG results in unequal filling of the bands with different spin projections. This leads to finite spin magnetization even in absence of external magnetic fields. This effect is known as Stoner instability [33]. In this work we investigate magnetic instabilities in 2D two-valley semiconductors in the presence of an in-plane magnetic field, valley SOI, and electron-electron interactions.

The valley degree of freedom together with the electron spin result in four single-particle bands, see Fig. 1. Thus, we have four different electron densities n_τ^λ , one per band, which are related to the corresponding chemical potentials. As the total electron density $n = \sum_{\lambda,\tau} n_\tau^\lambda$ is fixed by electrostatic gates, we have three independent magnetic order parameters which we can change. We make the following choice of the order parameters:

$$M_\beta = \sum_{\lambda,\tau} \frac{\lambda n_\tau^\lambda}{4\nu}, \quad M_v = \sum_{\lambda,\tau} \frac{\tau n_\tau^\lambda}{4\nu}, \quad M_{\beta v} = \sum_{\lambda,\tau} \frac{\lambda\tau n_\tau^\lambda}{4\nu}, \quad (5)$$

where $\nu = m/(2\pi)$ is the 2D density of states. All order parameters have dimension of energy. The order parameter M_v measures the valley magnetization, i.e. the imbalance between the electron density in different valleys. The combination $M_\beta + M_{\beta v}$ ($M_\beta - M_{\beta v}$) measures the spin magnetization in the $\tau = +1$ ($\tau = -1$) valley along the corresponding quantization axis given by the direction of the effective magnetic field $\boldsymbol{\beta}_+$ ($\boldsymbol{\beta}_-$), see Eq. (3). For example, the filling shown in Fig. 1 corresponds to $M_\beta \neq 0$, $M_v = M_{\beta v} = 0$.

Interaction matrix elements. We separate the interaction matrix elements into two groups. The first group

corresponds to the direct Coulomb interaction, v , describing the electrostatic coupling of electric charges:

$$v(q) = \nu \frac{2\pi e^2}{\epsilon q} = \frac{1}{qa_B}, \quad (6)$$

where we multiplied the Coulomb interaction by the 2D density of states $\nu = m/(2\pi)$, with m being the effective mass, $a_B = \epsilon/(me^2)$ the effective Bohr radius, and ϵ the dielectric constant. At small momentum transfers $q \lesssim k_F$, k_F being the Fermi momentum, the 2D Coulomb pole $1/q$ is screened by the electron-hole fluctuations giving rise to the Thomas-Fermi screening momentum $q_{TF} \sim 1/a_B$, see e.g. Ref. [34]:

$$v(q \lesssim k_F) \approx \frac{1}{(q + q_{TF})a_B}. \quad (7)$$

The regime of strong electron-electron interaction corresponds to low densities such that $k_F a_B \ll 1$. Thus, the $qa_B \lesssim k_F a_B \ll 1$ term is negligible compared to the $q_{TF} a_B \sim 1$ term in Eq. (7), which allows us to neglect the q -dependence in the direct interaction matrix element.

The second group of interaction matrix elements corresponds to the exchange intervalley interaction u . As the separation between the valleys is of the order of the Brillouin zone size, such an interaction is extremely short ranged and is mostly given by the on-site Hubbard term rather than by the long-range Coulomb interaction [34]. Here we treat the direct, v , and the intervalley exchange, u , matrix elements as free phenomenological parameters. We also assume that $u \ll v$, so we only account for the first order effects in u .

Magnetic phase diagram. Magnetic instabilities are typically studied within the self-consistent Born (SCB) approximation for the electron self-energy that accounts for the Fermi liquid renormalizations and the random phase approximation (RPA) for the dynamical screening of the Coulomb interaction [28]. Here, the RPA is motivated by a relatively large number of electron flavors due to the spin and valley quantum numbers [28]. In the static limit the RPA results in the Thomas-Fermi screening, see Eq. (7). Small dynamic corrections to the interaction which are not shown in Eq. (7) are responsible for the cubic non-analyticity in the free energy [28].

Neglecting the dynamical screening (i.e. treating u and v as constants) and applying the SCB approximation, we calculate the free energy of the two-valley 2DEG, see the Supplementary Material (SM) [35]:

$$F^{SCB} = 2\nu [a_\beta M_\beta^2 + a_v M_v^2 + a_{\beta v} M_{\beta v}^2 - 2\beta M_\beta], \quad (8)$$

where we subtracted the energy of the normal state. Here we introduced the Landau parameters:

$$a_\beta = 1 - v - \zeta u, \quad (9)$$

$$a_v = 1 - v + u, \quad (10)$$

$$a_{\beta v} = 1 - v + \zeta u, \quad (11)$$

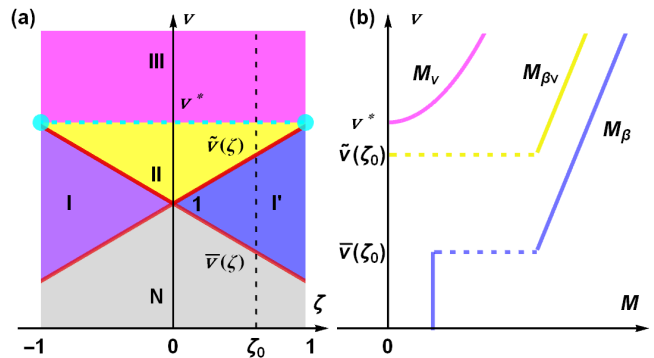


FIG. 2. (a) The magnetic phase diagram. The following phases are shown: the normal phase N (gray) with no condensed order parameters; the homogeneous phases I (purple) and I' (blue) with single condensed order parameter $M_{\beta v}$ and M_β , respectively; the phase II (yellow) with two condensed order parameters M_β and $M_{\beta v}$; the phase III (magenta) with non-zero ground state value of all three magnetic order parameters. The first (second) order phase transitions are shown by solid red (dashed red) lines. Two tri-critical points are indicated by cyan dots. The lines of phase transitions are given by Eqs. (13)–(15). (b) Schematic dependence of the order parameters along the cut $\zeta = \zeta_0$ on the phase diagram. Finite jump of M_β and $M_{\beta v}$ reflects the first order phase transitions, continuous dependence of M_v on v is due to the second order phase transition. Non-zero $M_\beta \propto \beta$ at $v < \bar{v}(\zeta_0)$ is due to finite external field β , see βM_β term in Eq. (8).

where

$$\zeta = \frac{b^2 - \alpha^2}{\beta^2} = \frac{b^2 - \alpha^2}{b^2 + \alpha^2}. \quad (12)$$

All order parameters are assumed to be much smaller than the Fermi energy $E_F = n/(4\nu)$ in the normal phase, n is the total density. The order parameter M_β is non-zero even in the normal phase due to the βM_β term, see Eq. (8), that results in small linear in $\beta \ll E_F$ polarization $M_\beta \propto \beta$. In what follows we assume that the spontaneous magnetization is always much larger than the finite field polarization $\propto \beta$, and, thus, we neglect the βM_β term. We only keep in mind that finite β explicitly breaks the $M_\beta \rightarrow -M_\beta$ symmetry of the free energy, and, thus, is responsible for the sign of M_β , which, however, is not important for our consideration.

Let us consider the case $1 > \zeta > 0$. In this case $a_v > a_{\beta v} > a_\beta$ at any $u > 0$ and $v > 0$. Starting from the normal phase at $v = 0$ and increasing the value of v we first find the phase transition for the order parameter M_β when $a_\beta = 0$, which corresponds to the following critical value of $v = \bar{v}(\zeta)$:

$$\bar{v}(\zeta) = 1 - \zeta u. \quad (13)$$

This corresponds to the phase transition from the normal phase (N) to the phase I' with condensed order parameter $M_\beta \neq 0$, see Fig. 2(a). Upon further increasing the

interaction parameter v , we find an instability for the $M_{\beta v}$ order parameter at $v = \tilde{v}(\zeta)$ at which $a_{\beta v} = 0$:

$$\tilde{v}(\zeta) = 1 + \zeta u. \quad (14)$$

This corresponds to the phase transition from the ordered phase I' with the only condensed order parameter $M_\beta \neq 0$ to the phase II with $M_\beta \neq 0$, $M_{\beta v} \neq 0$, $M_v = 0$. Increasing v even further, we reach the instability for the valley order parameter M_v when $a_v = 0$. This happens at $v = v^*$:

$$v^* = 1 + u. \quad (15)$$

This corresponds to the phase transition from the phase II to the phase III where all magnetic order parameters are condensed $M_\beta \neq 0$, $M_{\beta v} \neq 0$, $M_v \neq 0$. Further increase of the matrix element v does not result in additional instabilities within the SCB approximation, the system stays in the phase III at any $v > v^*$.

Similar analysis can be done for $\zeta < 0$. Upon increasing v from $v = 0$ we first find the instability for $M_{\beta v}$ at $v = \tilde{v}(\zeta) = 1 + \zeta u$, then the instability for M_β at $v = \bar{v}(\zeta) = 1 - \zeta u$, and then the instability for M_v at $v = v^* = 1 + u$. This results in the phase diagram shown in Fig. 2(a).

Order of phase transitions. Normally, the magnetic phase transitions are first order due to the non-analytic cubic correction to the free energy [36] that originates from the dynamical screening of the Coulomb interaction and from the interaction vertex correction [37] that are neglected within the SCB approximation. In the SM [35] we calculate the cubic correction within second order perturbation theory neglecting the u^2 term because we assume $u \ll v \sim 1$:

$$F^{cub} = -\frac{2\nu v^2}{3E_F} \left[\left(1 - \frac{2u}{v} \frac{b^2}{\beta^2} \right) f(M_v, M_{\beta v}) + \left(1 - \frac{2u}{v} \frac{\alpha^2}{\beta^2} \right) f(M_v, M_\beta) + f(M_\beta, M_{\beta v}) \right], \quad (16)$$

where $f(x, y) = f(y, x)$ is a symmetric non-analytic cubic function of two variables:

$$f(x, y) = |x|^3 + 3|x|y^2, \quad |x| \geq |y|. \quad (17)$$

Importantly, $f(x, y)$ is non-analytic only with respect to the largest in absolute value argument. This means that if all three order parameters are condensed, see phase III in Fig. 2(a), then the non-analyticity for the smallest order parameter is cut by larger ground state values of two other order parameters, see Eqs. (16) and (S51). As the Landau parameter a_v is always the largest, see Eqs. (9)–(11), then M_v order parameter is more suppressed compared to M_β and $M_{\beta v}$ i.e. $|M_v| < |M_\beta|$ and $|M_v| < |M_{\beta v}|$ in phase III. Therefore, there is no cubic in M_v term in the free energy. The absence of $|M_v|^3$ term results in the second order phase transition between phases II and III.

This is illustrated in Fig. 2(b) by the continuous dependence of M_v on v .

In all magnetic phases apart from the phase III $M_v = 0$, see Fig. 2(a). Therefore, in these phases $f(M_v, M_{\beta v}) = |M_{\beta v}|^3$, $f(M_v, M_\beta) = |M_\beta|^3$, i.e. the cubic non-analyticity for M_β and $M_{\beta v}$ is not cut in Eq. (16). As negative cubic non-analyticity necessarily leads to a first order phase transition [36], all other magnetic phase transitions are of the first order which is illustrated in Fig. 2(b) by the finite jumps of corresponding order parameters at the phase transition. For example, the first order ferromagnetic phase transition between normal phase and phase I at zero applied magnetic field, $\zeta = -1$, has been predicted in Ref. [11].

Due to finite external field β , M_β takes non-zero value $M_\beta \propto \beta$ even in normal phase which can be an issue for the experimental identification of phase I'. However, the discontinuity of M_β at the first order phase transition between normal phase and phase I' unambiguously signals the spontaneous symmetry breaking, see Fig. 2(b).

The zero temperature phase diagram shown in Fig. 2(a) contains two tri-critical points located at $v = v^*$ and $\zeta = \pm 1$ where the first and second order phase transition lines meet. The tri-critical points correspond to either zero magnetic field or zero SOI when all magnetic order parameters are Ising. We point out here that these tri-critical points have been overlooked in the previous theoretical studies [10, 11]. Second order phase transitions, see dashed cyan line $v = v^*$ in Fig. 2(a), and the tri-critical points result in quantum critical states that are characterized by emergent long range order and divergent susceptibilities [38]. Even though we predict these quantum critical points, we cannot describe them quantitatively within the mean field treatment that we use in this paper due to the increasingly important effect of the fermion fluctuations in the vicinity of such quantum critical points, for more information see Ref. [39].

Conclusions. In our study we predict a very rich magnetic phase diagram in 2D two-valley semiconductors with intrinsic valley SOI, in-plane magnetic field, and electron-electron interaction, see Fig. 2(a). Phase transitions between different phases can be driven by the electron density (varying the interaction parameter v) or by the external in-plane magnetic field. In spite of the cubic non-analytic corrections to the free energy that favors first order phase transitions, we showed that the phase transition between phases II and III, see Fig. 2(a), is second order. Together with two tri-critical points, the line of second order phase transitions constitute the quantum critical sector on the zero-temperature phase diagram.

Acknowledgments. This work was supported by the Georg H. Endress foundation, the Swiss National Science Foundation, and NCCR QSIT. This project received funding from the European Union's Horizon 2020 research and innovation program (ERC Starting Grant, grant agreement No 757725).

-
- [1] M. Dresselhaus, G. Dresselhaus, S. B. Cronin, A. G. S. Filho, *Solid State Properties: From Bulk to Nano* (Springer, Berlin, Heidelberg, ed. 1, 2018).
- [2] D. D. Awschalom, D. Loss, and N. Samarth (ed.), *Semiconductor Spintronics And Quantum Computation* (Springer Science and Business Media, 2013).
- [3] T. Ando, A. B. Fowler, F. Stern, *Rev. Mod. Phys.* **54**, 437 (1982).
- [4] D. Miserev, and O. P. Sushkov, *Phys. Rev. B* **100**, 205129 (2019).
- [5] N. W. Ashcroft and N. D. Mermin, *Solid State Physics* (Saunders, New York, 1974).
- [6] Q. H. Wang, K. Kalantar-Zadeh, A. Kis, J. N. Coleman, and M. S. Strano, *Nat. Nanotechnol.* **7**, 699–712 (2012).
- [7] X. Xu, W. Yao, D. Xiao, and T. F. Heinz, *Nat. Phys.* **10**, 343–350 (2014).
- [8] D. K. Mukherjee, A. Kundu, and H. A. Fertig, *Phys. Rev. B* **98**, 184413 (2018).
- [9] J. E. H. Braz, B. Amorim, and E. V. Castro, *Phys. Rev. B* **98**, 161406(R) (2018).
- [10] M. Van der Donck and F. M. Peeters, *Phys. Rev. B* **98**, 115432 (2018).
- [11] D. Miserev, J. Klinovaja, and D. Loss, *Phys. Rev. B* **100**, 014428 (2019).
- [12] A. Ramasubramaniam, *Phys. Rev. B* **86**, 115409 (2012).
- [13] T. Cheiwchanchamnangij and W. R. L. Lambrecht, *Phys. Rev. B* **85**, 205302 (2012).
- [14] W. Zhao, Z. Ghorannevis, L. Chu, M. Toh, C. Kloc, P.-H. Tan, and G. Eda, *ACS Nano* **7**, 791–797 (2012).
- [15] J. S. Ross, S. Wu, H. Yu, N. J. Ghimire, A. M. Jones, G. Aivazian, J. Yan, D. G. Mandrus, D. Xiao, W. Yao, and X. Xu, *Nat. Commun.* **4**, 1474 (2013).
- [16] E. S. Kadantsev and P. Hawrylak, *Solid State Commun.* **152**, 909913 (2012).
- [17] D. Xiao, G.-B. Liu, W. Feng, X. Xu, and W. Yao, *Phys. Rev. Lett.* **108**, 196802 (2012).
- [18] K. Kořmider, J. W. González, and J. Fernández-Rossier, *Phys. Rev. B* **88**, 245436 (2013).
- [19] G.-B. Liu, W.-Y. Shan, Y. Yao, W. Yao, and D. Xiao, *Phys. Rev. B* **88**, 085433 (2013).
- [20] J. Klinovaja and D. Loss, *Phys. Rev. B* **88**, 075404 (2013).
- [21] A. Kormányos, V. Zólyomi, N. D. Drummond, and G. Burkard, *Phys. Rev. X* **4**, 011034 (2014).
- [22] A. Kormányos, G. Burkard, M. Gmitra, J. Fabian, V. Zólyomi, N. D. Drummond, and V. Fal’ko, *2D Mater.* **2**, 022001 (2015).
- [23] D. Belitz, T. R. Kirkpatrick, and T. Vojta, *Rev. Mod. Phys.* **77**, 579 (2005).
- [24] J. G. Roch, G. Froehlicher, N. Leisgang, P. Makk, K. Watanabe, T. Taniguchi, and R. J. Warburton, *Nat. Nanotechnol.* **14**, 432–436 (2019).
- [25] J. G. Roch, D. Miserev, G. Froehlicher, N. Leisgang, L. Sponfeldner, K. Watanabe, T. Taniguchi, J. Klinovaja, D. Loss, and R. J. Warburton, *Phys. Rev. Lett.* **124**, 187602 (2020).
- [26] R. Pisoni, A. Kormányos, M. Brooks, Z. Lei, P. Back, M. Eich, H. Overweg, Y. Lee, P. Rickhaus, K. Watanabe, T. Taniguchi, A. Imamoglu, G. Burkard, T. Ihn, and K. Ensslin, *Phys. Rev. Lett.* **121**, 247701 (2018).
- [27] D. Belitz and T. R. Kirkpatrick, *Phys. Rev. Lett.* **89**, 247202 (2002).
- [28] D. L. Maslov and A. V. Chubukov, *Phys. Rev. B* **79**, 075112 (2009).
- [29] T. R. Kirkpatrick and D. Belitz, *Phys. Rev. B* **67**, 024419 (2003).
- [30] R. A. Zak, D. L. Maslov, and D. Loss, *Phys. Rev. B* **82**, 115415 (2010).
- [31] R. A. Zak, D. L. Maslov, and D. Loss, *Phys. Rev. B* **85**, 115424 (2012).
- [32] T. R. Kirkpatrick and D. Belitz, *Phys. Rev. Lett.* **124**, 147201 (2020).
- [33] E. C. Stoner, *Proc. R. Soc. Lond. A* **165**, 372–414 (1938).
- [34] R. Roldan, E. Cappelluti, and F. Guinea, *Phys. Rev. B* **88**, 054515 (2013).
- [35] See Supplemental Material at . . . for the derivation of the free energy including the interaction vertex correction and the dynamical screening of the Coulomb interaction.
- [36] D. Belitz, T. R. Kirkpatrick, and T. Vojta, *Phys. Rev. Lett.* **82**, 4707 (1999).
- [37] A. V. Chubukov, C. Pépin, and J. Rech, *Phys. Rev. Lett.* **92**, 147003 (2004).
- [38] S. Sachdev, *Quantum Phase Transitions* (Cambridge University Press, ed. 2, 2011).
- [39] H. v. Löhneysen, A. Rosch, M. Vojta, and P. Wölfle, *Rev. Mod. Phys.* **79**, 1015 (2007).
- [40] A. A. Abrikosov, L. P. Gorkov, and I. E. Dzialoshinskii, *Quantum Field Theoretical Methods in Statistical Physics* (Pergamon, 1965).

Supplemental Material for “Magnetic phase transitions in two-dimensional two-valley semiconductors with in-plane magnetic field ”

Dmitry Miserev, Jelena Klinovaja, and Daniel Loss

Department of Physics, University of Basel, Klingelbergstrasse 82, CH-4056 Basel, Switzerland

In the Supplemental Material (SM) we provide detailed calculations of the grand canonical potential Ω and the free energy F within the self-consistent Born (SCB) approximation for the electron self-energy and the random phase approximation (RPA) for the dynamically screened Coulomb potential. We first start from the non-interacting 2DEG. Then we account for the Fermi liquid renormalizations via the SCB approximation accounting for the Thomas-Fermi screening of the Coulomb interaction. Next we calculate the effect of the dynamical screening and the interaction vertex correction within second order perturbation theory which results in the cubic non-analyticity in the grand canonical potential. After that we perform the Legendre transformation in order to obtain the free energy which we analyze in the main text in terms of magnetic instabilities.

NON-INTERACTING 2DEG

Here we calculate the grand canonical potential for a non-interacting two-valley 2DEG with valley SOI and in-plane magnetic field. The effective single-particle Hamiltonian is given in Eqs. (1) and (2) in the main text. The electron spectrum is given by the twofold degenerate parabolic bands, see Eq. (4) in the main text. Here, we also require the electron spinors which explicitly show non-collinear spin quantization in different valleys:

$$|\lambda\tau\rangle = \frac{1}{\sqrt{2\beta(\beta - \alpha\lambda\tau)}} \begin{pmatrix} b_x - ib_y \\ \lambda(\beta - \alpha\lambda\tau) \end{pmatrix}, \quad (\text{S1})$$

where $\lambda = \pm 1$ is the eigenvalue of $\beta_\tau \cdot \boldsymbol{\sigma} / \beta$, $\tau = \pm 1$ labels the valley, α is the valley SOI, \mathbf{b} , β_τ , and β are defined in Eq. (3) in the main text. In what follows we also need the spinor overlap matrix elements:

$$M_{\tau\tau}^{\lambda'\lambda} = \langle \lambda'\tau | \lambda\tau \rangle = \delta^{\lambda'\lambda}, \quad (\text{S2})$$

$$M_{-\tau\tau}^{\lambda'\lambda} = \langle \lambda' - \tau | \lambda\tau \rangle = \frac{b}{\beta} \delta^{\lambda'\lambda} + \frac{\alpha\lambda\tau}{\beta} \delta^{-\lambda'\lambda}, \quad (\text{S3})$$

where δ^{ab} is the Kronecker symbol. The electron Matsubara Green function of the non-interacting 2DEG is diagonal in the basis of spinors $|\lambda\tau\rangle$, see Eq. (S1):

$$G(K) = \sum_{\lambda,\tau} |\lambda\tau\rangle \langle \lambda\tau | g_\tau^\lambda(K), \quad (\text{S4})$$

$$g_\tau^\lambda(K) = \frac{1}{i\omega - \varepsilon_0(k) + \lambda\beta + \mu_\tau^\lambda}, \quad (\text{S5})$$

where $K = (\mathbf{k}, \omega)$ is the “relativistic” notation for the momentum $\mathbf{k} = (k_x, k_y)$ and the Matsubara frequency ω , $\varepsilon_0(k) = k^2/2m$, μ_τ^λ are the chemical potentials. It is convenient to introduce the notation for chemical potentials $\tilde{\mu}_\tau^\lambda$ that are calculated from the bottom of the corresponding band:

$$\tilde{\mu}_\tau^\lambda = \mu_\tau^\lambda + \lambda\beta. \quad (\text{S6})$$

The non-interacting part of the grand canonical potential (per unit area) is given by the following expression:

$$\Omega_0 = \sum_{\lambda,\tau} \sum_K \ln [g_\tau^\lambda(K)], \quad (\text{S7})$$

where $\sum_K = T \sum_\omega \int d\mathbf{k} / (2\pi)^2$ ($\hbar = k_B = 1$). Evaluating the sum in Eq. (S7), we get

$$\Omega_0 = -\frac{\nu}{2} \sum_{\lambda,\tau} (\tilde{\mu}_\tau^\lambda)^2, \quad (\text{S8})$$

where $\nu = m/2\pi$ is the 2D density of states and m the effective mass.

SCB APPROXIMATION

In this section we calculate the effect of the Fermi liquid renormalization that we account for via the SCB approximation. Here we only account for the Thomas-Fermi screening of the Coulomb interaction that leads to effectively short-range interaction matrix elements v and u , v being the direct Coulomb interaction, $u \ll v$ the exchange intervalley interaction. For more information see the discussion in the main text after Eq. (6).

Within the SCB approximation, the self-energy is given by the diagrams in Fig. S1:

$$\begin{aligned} \Sigma_\tau^{\lambda\lambda'}(K) &= -\frac{v}{\nu} \sum_P \bar{g}_\tau^{\lambda\lambda'}(P) \\ &- \frac{u}{\nu} \sum_{\lambda_1, \lambda_2} \sum_P M_{\tau-\tau}^{\lambda\lambda_1} M_{-\tau\tau}^{\lambda_2\lambda'} \bar{g}_{-\tau}^{\lambda_1\lambda_2}(P), \end{aligned} \quad (\text{S9})$$

where the interaction is taken as contact interaction due to the Thomas-Fermi screening and the matrix elements $M_{\tau_1\tau_2}^{\lambda_1\lambda_2}$ are given by Eqs. (S2) and (S3). The Green function $\bar{g}_\tau^{\lambda\lambda'}(P)$ is self-consistently dressed by the self-energy:

$$\bar{g}_\tau(\omega, \mathbf{k}) = (i\omega - \varepsilon_0(k) + \tilde{\mu}_\tau - \Sigma_\tau)^{-1}, \quad (\text{S10})$$

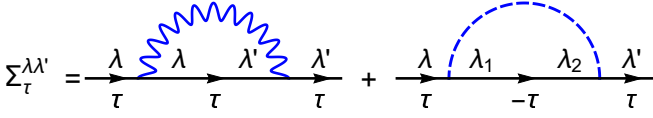


FIG. S1. The SCB approximation for the self-energy. Blue wavy (dashed) lines correspond to the v (u) components of the effective interaction. The black solid lines correspond to the electron Green function self-consistently dressed by the self-energy, see Eq. (S10).

where $\bar{g}_\tau(\omega, \mathbf{k})$ is a 2×2 matrix in the spin space, $\tilde{\mu}_\tau^{\lambda\lambda'} = \tilde{\mu}_\tau^\lambda \delta^{\lambda\lambda'}$, $\tilde{\mu}_\tau^\lambda$ is given by Eq. (S6). This is clear from Eq. (S9) that the exchange intervalley scattering u together with the non-collinearity of spins in different valleys breaks the valley spin conservation. The valley index of the single-particle Green function is conserved due to the momentum conservation because different valleys correspond to different momentum sectors.

Due to the contact approximation of the electron-electron interaction by constant matrix elements v and u , the self-energy, see Eq. (S9), does not depend on frequency and momentum. Therefore, the sum over momenta P in Eq. (S9) can be evaluated even for the dressed Green function:

$$\frac{1}{\nu} \sum_P \bar{g}_\tau^{\lambda\lambda'}(P) = \tilde{\mu}_\tau^\lambda \delta^{\lambda\lambda'} - \Sigma_\tau^{\lambda\lambda'} \equiv S_\tau^{\lambda\lambda'}, \quad (\text{S11})$$

where we introduced a new notation for convenience. Using Eq. (S11), we simplify the SCB Eq. (S9) to the following matrix equation:

$$S_\tau = \tilde{\mu}_\tau + v S_\tau + u M_{\tau-\tau} S_{-\tau} M_{-\tau\tau}, \quad (\text{S12})$$

where $\tilde{\mu}_\tau^{\lambda\lambda'} = \tilde{\mu}_\tau^\lambda \delta^{\lambda\lambda'}$, and the matrices $M_{-\tau\tau}$ and $M_{\tau-\tau}$ have spin matrix elements given by Eq. (S3). Changing $\tau \rightarrow -\tau$ in Eq. (S12), we get the second equation connecting S_τ and $S_{-\tau}$. The solution of Eq. (S12) is the following:

$$S_\tau = \frac{(1-v)\tilde{\mu}_\tau + u M_{\tau-\tau} \tilde{\mu}_{-\tau} M_{-\tau\tau}}{(1-v)^2 - u^2}. \quad (\text{S13})$$

In order to derive the grand canonical potential, we first calculate the following auxiliary energy functional [40]:

$$\Phi = \sum_{\lambda, \lambda', \tau} \sum_P \Sigma_\tau^{\lambda\lambda'} \bar{g}_\tau^{\lambda'\lambda}(P) = \nu \sum_{\lambda, \lambda', \tau} \Sigma_\tau^{\lambda\lambda'} S_\tau^{\lambda'\lambda}, \quad (\text{S14})$$

where we used Eq. (S11) to calculate the sum over P . Substituting Eq. (S13) into Eq. (S14), we find the Φ potential:

$$\begin{aligned} \Phi(v, u) = & -\nu \Phi_1(v, u) \sum_{\lambda, \tau} (\tilde{\mu}_\tau^\lambda)^2 \\ & -\nu \Phi_2(v, u) \sum_{\lambda, \tau} \left(\tilde{\mu}_\tau^\lambda \tilde{\mu}_{-\tau}^\lambda \frac{b^2}{\beta^2} + \tilde{\mu}_\tau^\lambda \tilde{\mu}_{-\tau}^{-\lambda} \frac{\alpha^2}{\beta^2} \right), \end{aligned} \quad (\text{S15})$$

where we introduced the following prefactors:

$$\Phi_1(v, u) = \frac{v(1-v)^2 + u^2(2-v)}{[(1-v)^2 - u^2]^2}, \quad (\text{S16})$$

$$\Phi_2(v, u) = \frac{u(1-v^2 + u^2)}{[(1-v)^2 - u^2]^2}. \quad (\text{S17})$$

The grand canonical potential is connected to the Φ potential through the following identity [40]:

$$\Omega = \Omega_0 + \frac{1}{2} \int_0^1 \frac{ds}{s} \Phi(sv, su), \quad (\text{S18})$$

where Ω_0 is given by Eq. (S8). Thus, we have to calculate the following elementary integrals:

$$\int_0^1 \frac{ds}{s} \Phi_1(sv, su) = \frac{v(1-v) + u^2}{(1-v)^2 - u^2}, \quad (\text{S19})$$

$$\int_0^1 \frac{ds}{s} \Phi_2(sv, su) = \frac{u}{(1-v)^2 - u^2}. \quad (\text{S20})$$

Substituting these integrals back into Eq. (S18), we find the grand canonical potential within the SCB approximation:

$$\begin{aligned} \Omega^{SCB} = & -\frac{\nu}{2} \frac{1}{(1-v)^2 - u^2} \sum_{\lambda, \tau} [(1-v)(\tilde{\mu}_\tau^\lambda)^2 \\ & + u \left(\frac{b^2}{\beta^2} \tilde{\mu}_\tau^\lambda \tilde{\mu}_{-\tau}^\lambda + \frac{\alpha^2}{\beta^2} \tilde{\mu}_\tau^\lambda \tilde{\mu}_{-\tau}^{-\lambda} \right)]. \end{aligned} \quad (\text{S21})$$

NON-ANALYTIC CUBIC CORRECTION

Within the SCB approximation we neglected the dynamic dependence of the Coulomb interaction and the interaction vertex correction. Here we account for these effects within second order perturbation expansion. It is well known that these effects give rise to the non-analytic cubic terms in the Ω potential [23, 27, 29, 32]. The diagrams that contribute to the cubic non-analyticity are shown in Fig. S2. In order to make the formal expressions corresponding to these diagrams more compact, we introduce the particle-hole bubble:

$$\Pi_{\tau\tau'}^{\lambda\lambda'}(Q) = \frac{1}{\nu} \sum_K g_\tau^\lambda(K) g_{\tau'}^{\lambda'}(K+Q). \quad (\text{S22})$$

The diagrams in Fig. S2(b),(d) do not appear in the SCB series and represent the renormalizations of the interaction vertex. However, the other two diagrams are partially accounted within the approximation that we have done in the previous section because we included the Thomas-Fermi screening of the Coulomb interaction. In order to avoid the double counting, we subtract the

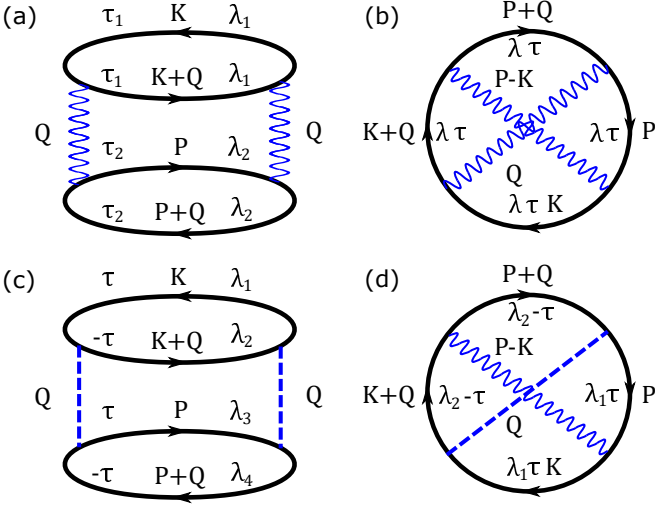


FIG. S2. Second order diagrams for the grand canonical potential Ω beyond the SCB approximation. Blue wavy (dashed) line corresponds to the v (u) component of the effective interaction. The black solid lines correspond to the bare electron Green function, see Eq. (S5).

static part of the particle-hole bubbles that is responsible for the Thomas-Fermi screening from the diagrams in Fig. S2(a),(c). In other words, we only account for the dynamic part of the screened Coulomb interaction in Fig. S2(a),(c). As we are interested in the lowest order perturbation correction to the cubic non-analyticity, we also neglect the Fermi liquid renormalizations, i.e. the Green functions in the diagrams in Fig. S2 are assumed to be bare, see Eq. (S5).

The diagrams in Fig. S2 have the following analytic representations:

$$\Omega_a = -\frac{v^2}{4} \sum_{\tau_1, \tau_2} \sum_{\lambda_1, \lambda_2} \sum_Q \Pi_{\tau_1 \tau_1}^{\lambda_1 \lambda_1}(Q) \Pi_{\tau_2 \tau_2}^{\lambda_2 \lambda_2}(Q), \quad (\text{S23})$$

$$\Omega_b = \frac{v^2}{4} \sum_{\tau, \lambda} \sum_Q \left[\Pi_{\tau \tau}^{\lambda \lambda}(Q) \right]^2, \quad (\text{S24})$$

$$\Omega_c = -\frac{u^2}{4} \sum_{\tau, \lambda_i, Q} |M_{\tau-\tau}^{\lambda_1 \lambda_2} M_{\tau-\tau}^{\lambda_3 \lambda_4}|^2 \Pi_{\tau-\tau}^{\lambda_1 \lambda_2}(Q) \Pi_{\tau-\tau}^{\lambda_3 \lambda_4}(Q), \quad (\text{S25})$$

$$\Omega_d = 2\frac{uv}{4} \sum_{\tau, \lambda_1, \lambda_2} \sum_Q |M_{\tau-\tau}^{\lambda_1 \lambda_2}|^2 \left[\Pi_{\tau-\tau}^{\lambda_1 \lambda_2}(Q) \right]^2, \quad (\text{S26})$$

where $\nu = m/2\pi$ is the 2D density of states, m is the effective mass. We note the additional factor of 2 in Ω_d . This is because Ω_d is represented by two diagrams: one is shown in Fig. S2(d) and the other is different by swapping dashed and wavy interaction lines.

The non-analyticity in Ω comes from the non-analyticities of the particle-hole bubble $\Pi_{\tau \tau}^{\lambda \lambda'}(Q)$, $Q = (\mathbf{q}, \varepsilon)$, which are known as Landau damping at $Q \approx 0$ and Kohn anomaly at $q = 2k_F$, $\varepsilon = 0$, and k_F is the Fermi momentum [28]. First, we find the Landau damp-

ing contribution using the following approximation of the particle-hole bubble at small $Q = (\mathbf{q}, \varepsilon)$, see e.g. Refs. [30, 31]:

$$\Pi_{\tau \tau'}^{\lambda \lambda'}(\mathbf{q}, \varepsilon) \approx \frac{|\varepsilon|}{\sqrt{(\varepsilon - i\Delta_{\tau \tau'}^{\lambda \lambda'})^2 + (v_F q)^2}} - 1, \quad (\text{S27})$$

where $v_F = k_F/m$ is the Fermi velocity and

$$\Delta_{\tau \tau'}^{\lambda \lambda'} = \tilde{\mu}_\tau^\lambda - \tilde{\mu}_{\tau'}^{\lambda'}. \quad (\text{S28})$$

It is assumed here that $\Delta_{\tau \tau'}^{\lambda \lambda'} \ll \tilde{\mu}_\tau^\lambda, \tilde{\mu}_{\tau'}^{\lambda'}$. Then, the calculation of any sum which is quadratic with respect to the particle-hole bubble is straightforward and can be found e.g. in Ref. [11]:

$$\sum_Q^L \Pi_{\tau_1 \tau_2}^{\lambda_1 \lambda_2}(Q) \Pi_{\tau_3 \tau_4}^{\lambda_3 \lambda_4}(Q) = \frac{\nu T^3}{4E_F} \mathcal{F} \left(\frac{\Delta_{\tau_1 \tau_2}^{\lambda_1 \lambda_2} + \Delta_{\tau_3 \tau_4}^{\lambda_3 \lambda_4}}{2T} \right) \quad (\text{S29})$$

where the index L of the sum indicates that Q is in the vicinity of the Landau damping point. The function $\mathcal{F}(z)$ has the following integral representation:

$$\mathcal{F}(z) = \int_0^z dx x^2 \coth \left(\frac{x}{2} \right). \quad (\text{S30})$$

At small temperature $T \rightarrow 0$ the argument of \mathcal{F} in Eq. (S29) is large and one can use the asymptotic expansion:

$$\mathcal{F}(z) = \frac{|z|^3}{3} + 4\zeta(3) + O(e^{-|z|}), \quad |z| \gg 1, \quad (\text{S31})$$

where $\zeta(z)$ is the Riemann ζ -function. The function $\mathcal{F}(z)$ results in the cubic non-analyticity of the Ω potential.

The Kohn anomaly contribution can be reduced to the Landau damping with the help of a trick used in Refs. [11, 28]:

$$\sum_Q^K \Pi_{\tau_1 \tau_2}^{\lambda_1 \lambda_2}(Q) \Pi_{\tau_3 \tau_4}^{\lambda_3 \lambda_4}(Q) = \frac{\nu T^3}{4E_F} \mathcal{F} \left(\frac{\Delta_{\tau_1 \tau_3}^{\lambda_1 \lambda_3} + \Delta_{\tau_2 \tau_4}^{\lambda_2 \lambda_4}}{2T} \right). \quad (\text{S32})$$

Therefore, the total non-analytic contribution coming from both the Landau damping and the Kohn anomalies of the particle-hole bubbles can be combined into the following expression:

$$\sum_Q \Pi_{\tau_1 \tau_2}^{\lambda_1 \lambda_2}(Q) \Pi_{\tau_3 \tau_4}^{\lambda_3 \lambda_4}(Q) = \frac{\nu T^3}{4E_F} \times \left[\mathcal{F} \left(\frac{\Delta_{\tau_1 \tau_2}^{\lambda_1 \lambda_2} + \Delta_{\tau_3 \tau_4}^{\lambda_3 \lambda_4}}{2T} \right) + \mathcal{F} \left(\frac{\Delta_{\tau_1 \tau_3}^{\lambda_1 \lambda_3} + \Delta_{\tau_2 \tau_4}^{\lambda_2 \lambda_4}}{2T} \right) \right] \quad (\text{S33})$$

Using Eq. (S33) and the expansion (S31) we get the non-analytic parts of the diagrams in Fig. S2 at zero tem-

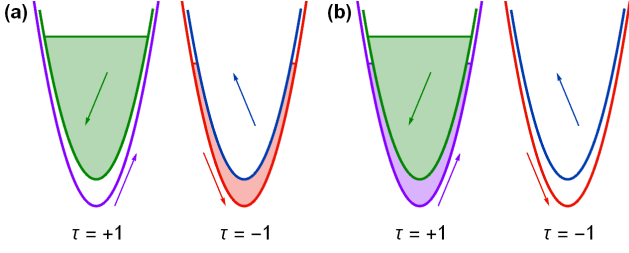


FIG. S3. Illustration of the band filling that corresponds to (a) $M_{\beta v} \neq 0$, $M_{\beta} = M_v = 0$; (b) $M_v \neq 0$, $M_{\beta} = M_{\beta v} = 0$. Example of the band filling corresponding to $M_{\beta} \neq 0$, $M_{\beta v} = M_v = 0$ is shown in Fig. 1 in the main text.

perature $T = 0$:

$$\delta\Omega_a = -\frac{\nu v^2}{48E_F} \sum_{\tau_1, \tau_2} \sum_{\lambda_1, \lambda_2} |\Delta_{\tau_1, \tau_2}^{\lambda_1 \lambda_2}|^3, \quad (\text{S34})$$

$$\delta\Omega_b = 0, \quad (\text{S35})$$

$$\delta\Omega_c = -\frac{\nu u^2}{48E_F} \sum_{\tau, \lambda_1, \lambda_2} \quad (\text{S36})$$

$$\begin{aligned} & \times \left[\frac{b^4}{8\beta^4} \left(|\Delta_{\tau-\tau}^{\lambda_1 \lambda_1} + \Delta_{\tau-\tau}^{\lambda_2 \lambda_2}|^3 + |\Delta_{\tau\tau}^{\lambda_1 \lambda_2} + \Delta_{-\tau-\tau}^{\lambda_1 \lambda_2}|^3 \right) \right. \\ & + \frac{\alpha^4}{8\beta^4} \left(|\Delta_{\tau-\tau}^{\lambda_1 - \lambda_1} + \Delta_{\tau-\tau}^{\lambda_2 - \lambda_2}|^3 + |\Delta_{\tau\tau}^{\lambda_1 \lambda_2} + \Delta_{-\tau-\tau}^{-\lambda_1 - \lambda_2}|^3 \right), \\ & \left. + \frac{\alpha^2 b^2}{4\beta^4} \left(|\Delta_{\tau-\tau}^{\lambda_1 \lambda_1} + \Delta_{\tau-\tau}^{\lambda_2 - \lambda_2}|^3 + |\Delta_{\tau\tau}^{\lambda_1 \lambda_2} + \Delta_{-\tau-\tau}^{\lambda_1 - \lambda_2}|^3 \right) \right], \\ \delta\Omega_d & = \frac{\nu uv}{24E_F} \sum_{\tau, \lambda} \left[\frac{b^2}{\beta^2} |\Delta_{\tau-\tau}^{\lambda \lambda}|^3 + \frac{\alpha^2}{\beta^2} |\Delta_{\tau-\tau}^{\lambda - \lambda}|^3 \right]. \quad (\text{S37}) \end{aligned}$$

LEGENDRE TRANSFORM AND FREE ENERGY

Here we calculate the free energy per unit area using the Legendre transform:

$$\begin{aligned} F & = \Omega - \sum_{\lambda, \tau} \mu_{\tau}^{\lambda} \frac{\partial \Omega}{\partial \mu_{\tau}^{\lambda}} = \\ \Omega & + \sum_{\lambda, \tau} \mu_{\tau}^{\lambda} n_{\tau}^{\lambda} = \Omega + \sum_{\lambda, \tau} \tilde{\mu}_{\tau}^{\lambda} n_{\tau}^{\lambda} - \beta \sum_{\lambda, \tau} \lambda n_{\tau}^{\lambda}, \quad (\text{S38}) \end{aligned}$$

where n_{τ}^{λ} is the density of electrons corresponding to the band with indices λ and τ . The total density is controlled by external gates and, thus, is constant. In the main text we define the following order parameters:

$$M_{\beta} = \sum_{\lambda, \tau} \frac{\lambda n_{\tau}^{\lambda}}{4\nu}, \quad M_v = \sum_{\lambda, \tau} \frac{\tau n_{\tau}^{\lambda}}{4\nu}, \quad M_{\beta v} = \sum_{\lambda, \tau} \frac{\lambda \tau n_{\tau}^{\lambda}}{4\nu} \quad (\text{S39})$$

Examples of the filling corresponding to non-zero values of one of these order parameters are shown in Fig. 1 in the main text and in Fig. S3. The electron densities n_{τ}^{λ} can be expressed in terms of these order parameters and

the total density n :

$$n_{+}^{+} = \nu (M_{\beta} + M_v + M_{\beta v}) + \frac{n}{4}, \quad (\text{S40})$$

$$n_{-}^{+} = \nu (M_{\beta} - M_v - M_{\beta v}) + \frac{n}{4}, \quad (\text{S41})$$

$$n_{+}^{-} = \nu (-M_{\beta} + M_v - M_{\beta v}) + \frac{n}{4}, \quad (\text{S42})$$

$$n_{-}^{-} = \nu (-M_{\beta} - M_v + M_{\beta v}) + \frac{n}{4}. \quad (\text{S43})$$

Since the order parameters are assumed to be much smaller than E_F , the densities n_{τ}^{λ} are all well-defined and non-negative. We use these relations to calculate the following sums:

$$\sum_{\lambda, \tau} (n_{\tau}^{\lambda})^2 = \frac{n^2}{4} + 4\nu^2 (M_{\beta}^2 + M_v^2 + M_{\beta v}^2), \quad (\text{S44})$$

$$\sum_{\lambda, \tau} n_{\tau}^{\lambda} n_{-\tau}^{\lambda} = \frac{n^2}{4} + 4\nu^2 (M_{\beta}^2 - M_v^2 - M_{\beta v}^2), \quad (\text{S45})$$

$$\sum_{\lambda, \tau} n_{\tau}^{\lambda} n_{\tau}^{-\lambda} = \frac{n^2}{4} + 4\nu^2 (-M_{\beta}^2 + M_v^2 - M_{\beta v}^2), \quad (\text{S46})$$

$$\sum_{\lambda, \tau} n_{\tau}^{\lambda} n_{-\tau}^{-\lambda} = \frac{n^2}{4} + 4\nu^2 (-M_{\beta}^2 - M_v^2 + M_{\beta v}^2), \quad (\text{S47})$$

$$\sum_{\lambda, \tau} |n_{\tau}^{\lambda} - n_{\tau}^{-\lambda}|^3 = 32\nu^3 f(M_{\beta}, M_{\beta v}), \quad (\text{S48})$$

$$\sum_{\lambda, \tau} |n_{\tau}^{\lambda} - n_{-\tau}^{\lambda}|^3 = 32\nu^3 f(M_v, M_{\beta v}), \quad (\text{S49})$$

$$\sum_{\lambda, \tau} |n_{\tau}^{\lambda} - n_{-\tau}^{-\lambda}|^3 = 32\nu^3 f(M_{\beta}, M_v), \quad (\text{S50})$$

where we introduced the following symmetric function:

$$f(x, y) = \frac{1}{2} (|x + y|^3 + |x - y|^3). \quad (\text{S51})$$

We calculated the grand canonical potential within the SCB approximation, see Eq. (S21), and also included small cubic corrections coming from the dynamical screening of the Coulomb interaction and the interaction vertex correction, see Eqs. (S34)–(S37):

$$\Omega = \Omega^{SCB} + \delta\Omega, \quad (\text{S52})$$

$$\delta\Omega = \delta\Omega_a + \delta\Omega_b + \delta\Omega_c + \delta\Omega_d, \quad (\text{S53})$$

where $\delta\Omega$ is the total cubic correction.

Let us first set $\delta\Omega$ to zero and calculate the SCB contribution to the free energy. The electron densities are given by derivatives of Ω^{SCB} , see Eq. (S21), with respect to the chemical potentials:

$$\begin{aligned} n_{\tau}^{\lambda} & = -\frac{\partial \Omega^{SCB}}{\partial \mu_{\tau}^{\lambda}} = \frac{\nu}{(1-\nu)^2 - u^2} [(1-\nu)\tilde{\mu}_{\tau}^{\lambda} \\ & + u \left(\frac{b^2}{\beta^2} \tilde{\mu}_{-\tau}^{\lambda} + \frac{\alpha^2}{\beta^2} \tilde{\mu}_{-\tau}^{-\lambda} \right)]. \quad (\text{S54}) \end{aligned}$$

This is the linear relation which can be inverted exactly:

$$\nu\tilde{\mu}_\tau^\lambda = \frac{1-v}{(1-v)^2 - \zeta^2 u^2} \left\{ \left[(1-v)^2 - \frac{u^2}{2}(1+\zeta^2) \right] n_\tau^\lambda + \frac{u^2}{2}(1-\zeta^2)n_\tau^{-\lambda} \right\} - \frac{u}{(1-v)^2 - \zeta^2 u^2} \left\{ \frac{1+\zeta}{2} [(1-v)^2 - \zeta u^2] n_{-\tau}^\lambda + \frac{1-\zeta}{2} [(1-v)^2 + \zeta u^2] n_{-\tau}^{-\lambda} \right\}, \quad (\text{S55})$$

where

$$\zeta = \frac{b^2 - \alpha^2}{\beta^2} = \frac{b^2 - \alpha^2}{b^2 + \alpha^2}. \quad (\text{S56})$$

Here we assume $u \ll v$ and expand Eq. (S55) with respect to u leaving only the first order terms in u , while v is treated non-perturbatively:

$$\nu\tilde{\mu}_\tau^\lambda \approx (1-v)n_\tau^\lambda - \frac{u}{2} [(1+\zeta)n_{-\tau}^\lambda + (1-\zeta)n_{-\tau}^{-\lambda}]. \quad (\text{S57})$$

The SCB contribution to the free energy then reads:

$$F^{SCB} = \Omega^{SCB} + \sum_{\lambda,\tau} \tilde{\mu}_\tau^\lambda n_\tau^\lambda - 4\nu\beta M_\beta = \frac{1}{2} \sum_{\lambda,\tau} \tilde{\mu}_\tau^\lambda n_\tau^\lambda - 4\nu\beta M_\beta. \quad (\text{S58})$$

Here we used the following identity:

$$\sum_{\lambda,\tau} \tilde{\mu}_\tau^\lambda n_\tau^\lambda = -2\Omega^{SCB}, \quad (\text{S59})$$

where the factor 2 comes from the quadratic scaling of Ω^{SCB} with the chemical potentials. Substituting the chemical potentials given by Eq. (S57) into Eq. (S58), we find the SCB contribution to the free energy:

$$F^{SCB} = \frac{1-v}{2\nu} \sum_{\lambda,\tau} (n_\tau^\lambda)^2 - 4\nu\beta M_\beta - \frac{u}{4\nu} \sum_{\lambda,\tau} [(1+\zeta)n_\tau^\lambda n_{-\tau}^\lambda + (1-\zeta)n_\tau^\lambda n_{-\tau}^{-\lambda}]. \quad (\text{S60})$$

Finally, we use the sums given in Eqs. (S44)–(S47) in order to represent the free energy in terms of the order parameters given by Eq. (S39). This gives Eq. (8) in the main text.

Next, we calculate the cubic correction to the free energy. From Eq. (S38), we find the correction to the free energy:

$$\delta F = \delta\Omega + \delta\Omega^{SCB} + \sum_{\lambda,\tau} \delta\tilde{\mu}_\tau^\lambda n_\tau^\lambda, \quad (\text{S61})$$

where $\delta\Omega$ is the cubic correction, see Eq. (S53), $\delta\Omega^{SCB}$ comes from the change in the chemical potentials:

$$\delta\Omega^{SCB} = \sum_{\lambda,\tau} \frac{\partial\Omega^{SCB}}{\partial\mu_\tau^\lambda} \delta\tilde{\mu}_\tau^\lambda = - \sum_{\lambda,\tau} (n_\tau^\lambda - \delta n_\tau^\lambda) \delta\tilde{\mu}_\tau^\lambda \approx - \sum_{\lambda,\tau} n_\tau^\lambda \delta\tilde{\mu}_\tau^\lambda, \quad (\text{S62})$$

where we used that $\Omega^{SCB} = \Omega - \delta\Omega$, see Eq. (S52), $\delta n_\tau^\lambda = -\partial\delta\Omega/\partial\mu_\tau^\lambda$ is the non-analytic contribution to the densities. Substituting Eq. (S62) back into Eq. (S61), we get the non-analytic correction to the free energy:

$$\delta F = \delta\Omega(\tilde{\mu}_\tau^\lambda = n_\tau^\lambda/\nu), \quad (\text{S63})$$

where we used the relation $\tilde{\mu}_\tau^\lambda = n_\tau^\lambda/\nu$ that is true in the non-interacting 2DEG because the cubic correction $\delta\Omega$, see Eq. (S53), was calculated within second order perturbation theory. Including the interaction corrections in $\tilde{\mu}_\tau^\lambda$ is beyond the applicability of the approximation that we used. As we neglected the u^2 terms in the SCB approximation, see Eq. (S57), we have to do the same with the cubic correction, i.e. we neglect $\delta\Omega_c$, see Eq. (S36). Thus, the cubic correction is given by Eqs. (S34), (S37) and can be simplified using $\tilde{\mu}_\tau^\lambda = n_\tau^\lambda/\nu$ and the sums given by Eqs. (S48)–(S50). This results in Eq. (16) in the main text.